Figure 1.

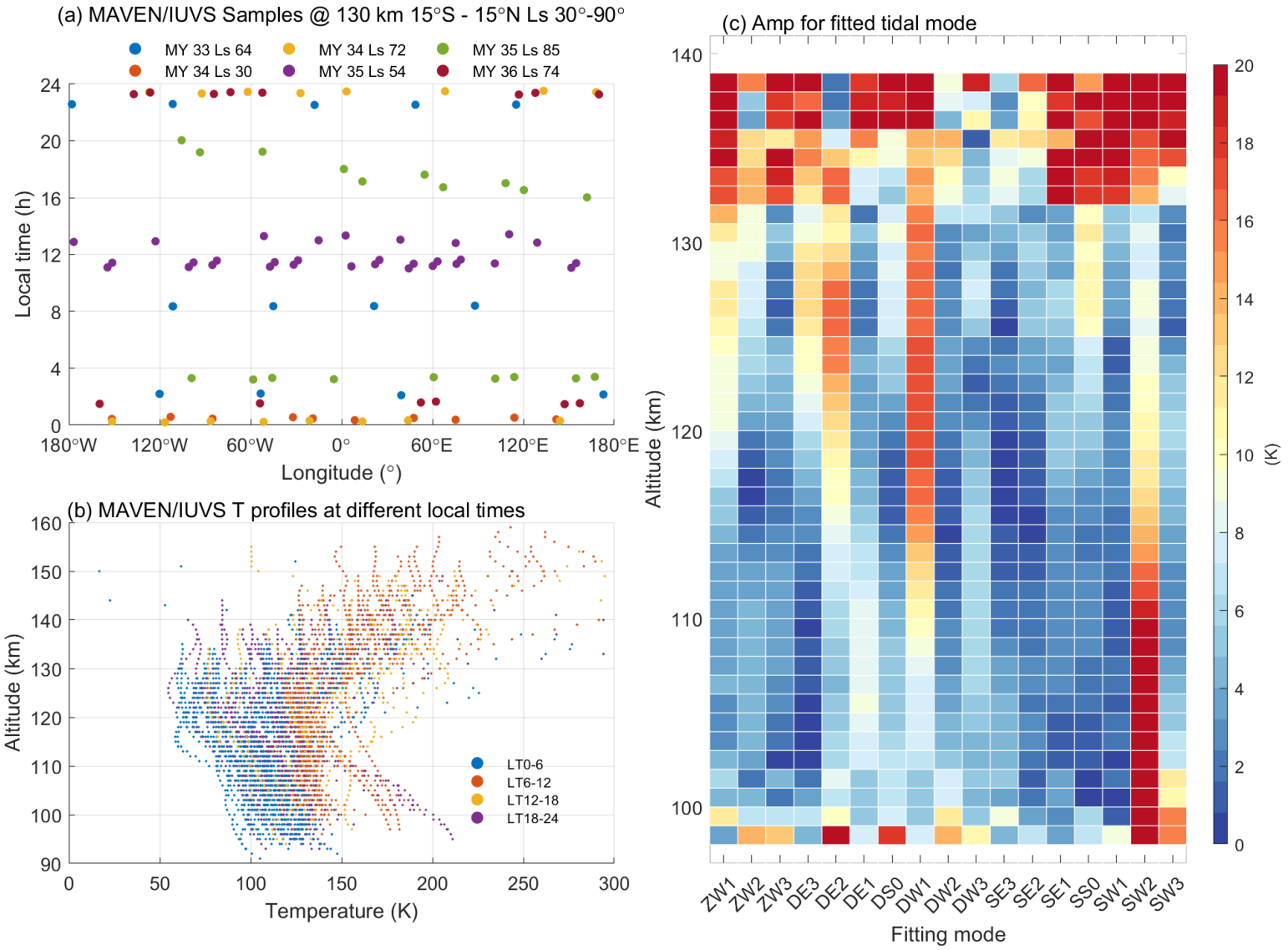
(a) MAVEN/IUVS Samples @ 130 km 15°S - 15°N Ls 30°-90°
MY 33 Ls 64
MY 34 Ls 30
MY 34 Ls 72
MY 35 Ls 54
MY 35 Ls 85
MY 36 Ls 74
Local time (h)
Longitude (°)
180°W
120°W
60°W
0°
60°E
120°E
180°E
(b) MAVEN/IUVS T profiles at different local times
Altitude (km)
Temperature (K)
LT0-6
LT6-12
LT12-18
LT18-24
(c) Amp for fitted tidal mode
Altitude (km)
Fitting mode
ZW1
ZW2
ZW3
DE3
DE2
DE1
DS0
DW1
DW2
DW3
SE3
SE2
SE1
SS0
SW1
SW2
SW3
(K)

Figure 2.

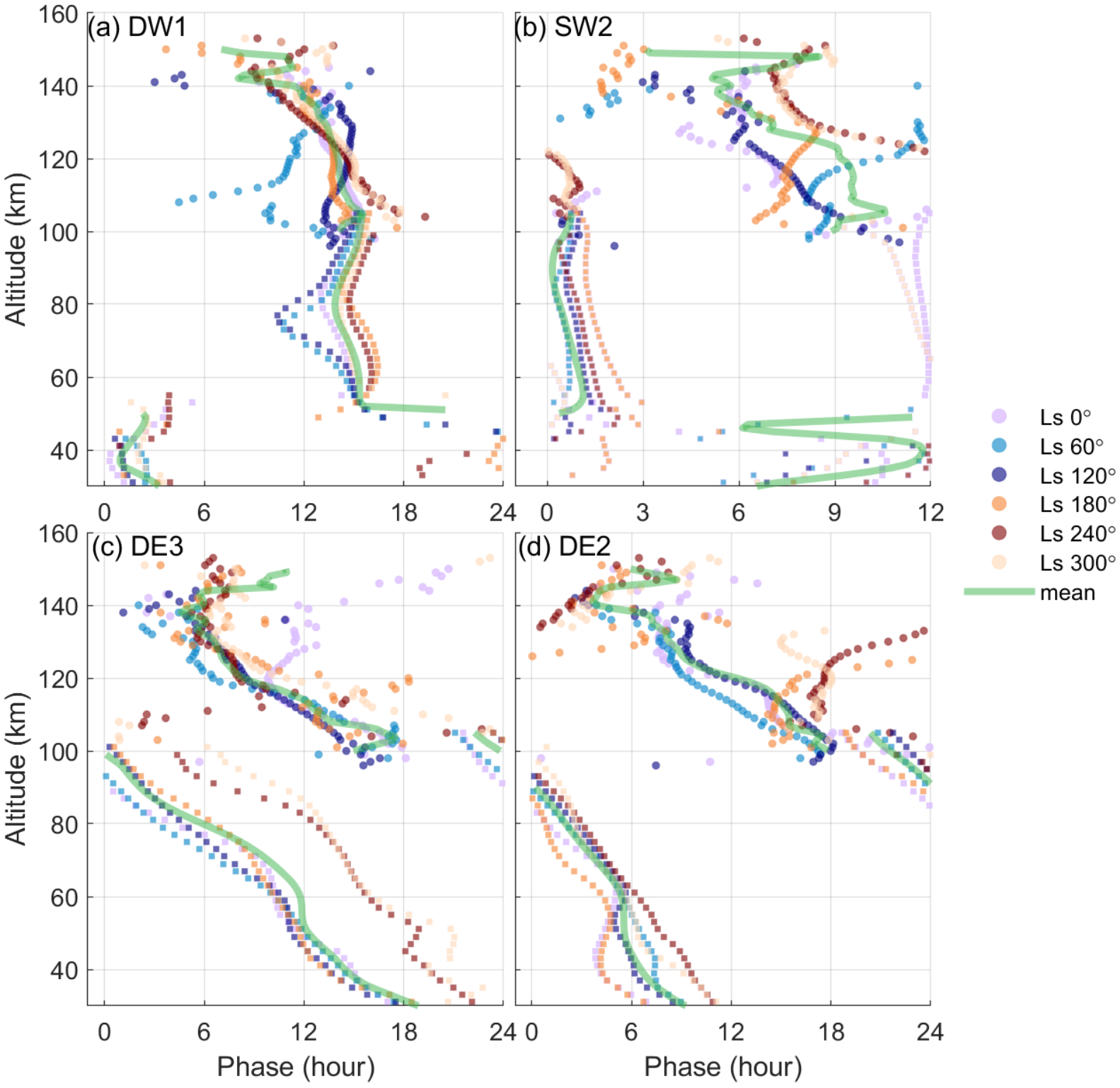
(a) DW1
(b) SW2
(c) DE3
(d) DE2
Altitude (km)
Phase (hour)
160
140
120
100
80
60
40
0
6
12
18
24
3
9
Ls 0°
Ls 60°
Ls 120°
Ls 180°
Ls 240°
Ls 300°
mean

Figure 3.

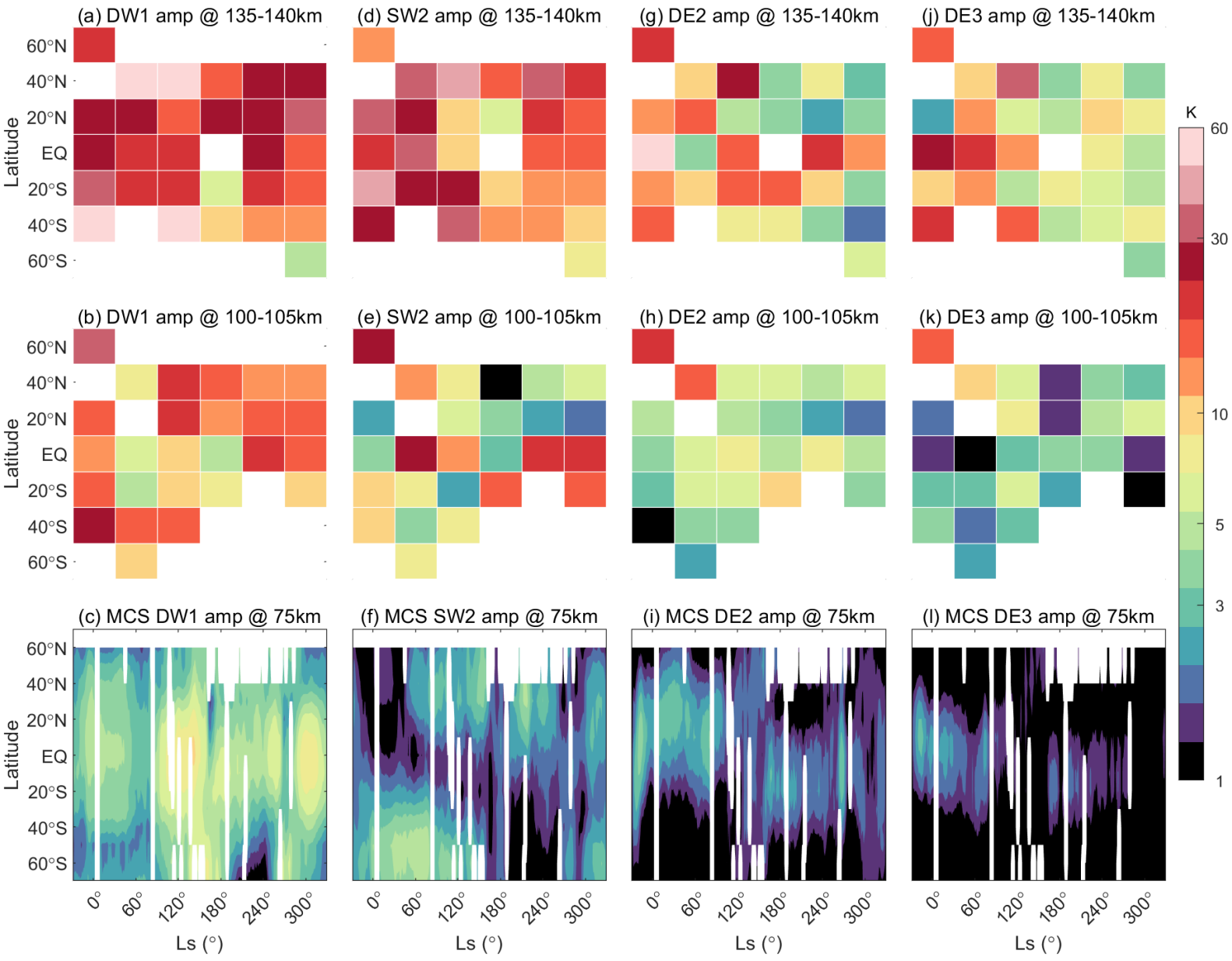
(a) DW1 amp @ 135-140km
(d) SW2 amp @ 135-140km
(g) DE2 amp @ 135-140km
(j) DE3 amp @ 135-140km
(b) DW1 amp @ 100-105km
(e) SW2 amp @ 100-105km
(h) DE2 amp @ 100-105km
(k) DE3 amp @ 100-105km
(c) MCS DW1 amp @ 75km
(f) MCS SW2 amp @ 75km
(i) MCS DE2 amp @ 75km
(l) MCS DE3 amp @ 75km
Latitude
60°N
40°N
20°N
EQ
20°S
40°S
60°S
0°
60°
120°
180°
240°
300°
Ls (°)
K
60
30
10
5
3
1

Figure 4.

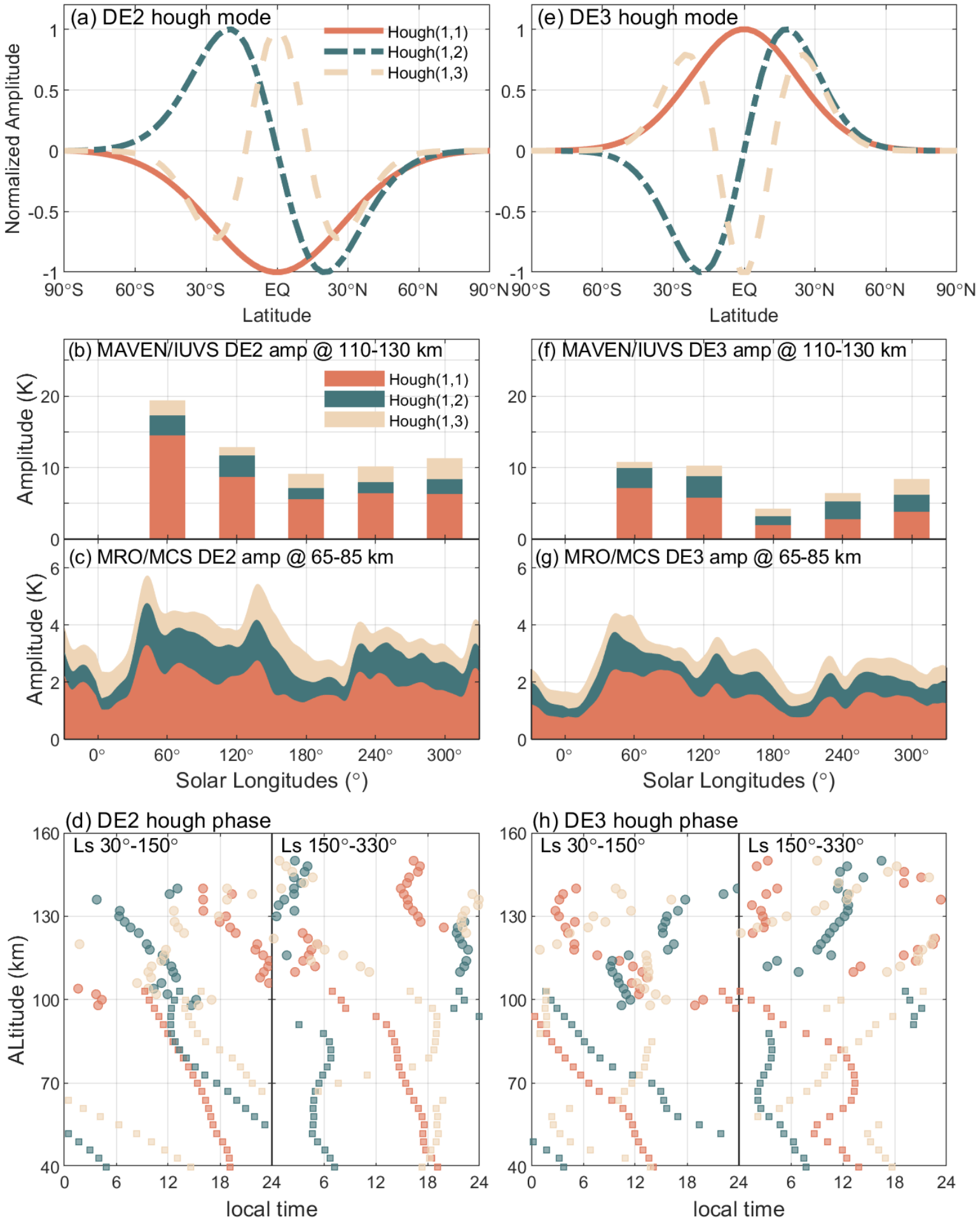
(a) DE2 hough mode
Hough(1,1)
Hough(1,2)
Hough(1,3)
Normalized Amplitude
Latitude
(e) DE3 hough mode
(b) MAVEN/IUVS DE2 amp @ 110-130 km
Amplitude (K)
(f) MAVEN/IUVS DE3 amp @ 110-130 km
(c) MRO/MCS DE2 amp @ 65-85 km
Solar Longitudes (°)
(g) MRO/MCS DE3 amp @ 65-85 km
(d) DE2 hough phase
Ls 30°-150°
Ls 150°-330°
ALtitude (km)
local time
(h) DE3 hough phase

Martian atmospheric tides revealed from MAVEN/IUVS and MRO/MCS Observations

Chengyun Yang[1,2], Tao Li*[1,2], Mengzhen Yuan[1], Zhaopeng Wu[3] and Xin Fang[1,2]

[1] CAS Key Laboratory of Geospace Environment, School of Earth and Space Sciences, University of Science and Technology of China, Hefei, China.

[2] CAS Center for Excellence in Comparative Planetology, University of Science and Technology of China, Hefei, China.

[3] Key Laboratory of Earth and Planetary Physics, Institute of Geology and Geophysics, Chinese Academy of Sciences, Beijing, China.

Corresponding author: Tao Li, litao@ustc.edu.cn

Key Points:

- The thermal tides are derived from temperature observations by two satellites with different altitude ranges.
- Migrating tides are strong in the mesosphere and thermosphere and can propagate above 100 km during the Martian dust season.
- During non-dust season, the diurnal eastward wavenumber 2 (DE2) and 3 (DE3) tides propagate upward from the troposphere to the thermosphere.

Abstract

Utilizing atmospheric temperature observed from Mars Years 33 to 36 by the Imaging Ultraviolet Spectrograph (IUVS) onboard the Mars Atmosphere and Volatile Evolution (MAVEN) and Mars Climate Sounder (MCS) onboard Mars Reconnaissance Orbiter (MRO), we derive the diurnal and semidiurnal thermal tides from 30 to 160 km. Vertical phase velocities of the migrating tides indicate their upward propagation above 100 km during the dust season (solar longitude, Ls 240° to 300°). During the non-dust season (Ls 30° to 150°), the diurnal eastward wavenumber 2 (DE2) and wavenumber 3 (DE3) tides can propagate upward from the lower atmosphere to ~140 km. The seasonal variation of DE2 and DE3 amplitudes in the thermosphere corresponds well to their counterparts in the lower atmosphere, primarily controlled by their Hough (1,1) modes. The upward propagation of these tides could potentially impact the vertical coupling between the Martian lower and upper atmosphere.

Plain Language Summary

Atmospheric thermal tides are perturbations caused by the absorption of solar radiation in the atmosphere, a phenomenon in Earth's and other planetary atmospheres. The vertical propagation of tides plays a crucial role in transporting energy and momentum vertically within the atmosphere. Observing atmospheric temperatures at different local times makes it possible to determine various tidal components' amplitude and propagation characteristics. Based on data from different satellites, this study investigates the characteristics of tidal amplitude and propagation on Mars. The migrating tides, which move westward in sync with the sun's motion, can propagate upward in the region above 100 km during the dust season. During the non-dust season on Mars, the diurnal eastward propagating wavenumber 2 (DE2) and wavenumber 3 (DE3) tide exhibits apparent upward propagation from the atmosphere below 40 km into the thermosphere. As Mars has weaker gravity and a lower exobase altitude than Earth, the vertical propagation of tides may directly transmit energy from lower atmospheric activities to the upper layers of the Martian atmosphere, influencing the atmospheric escape rate.

1 Introduction

As planetary-scale gravity internal waves, atmospheric solar tides can significantly influence diurnal and semidiurnal variations of the Martian atmosphere's density, temperature, pressure, and wind (Chapman & Lindzen, 1987; Forbes, 2013; Forbes et al., 2020). Given their characteristics of vertical propagation and tendency to grow with height, atmospheric tides play a crucial role in transporting momentum and energy from the lower to the upper atmosphere, even to the edge of space (Angelats I Coll et al., 2004; England et al., 2016, 2019; Forbes et al., 2002; Moudden & Forbes, 2015). Characterized by a zonally symmetric structure fixed in local time (LT), the migrating thermal tide moves westward in sync with the sun's motion (Forbes, 2004). On the other hand, nonmigrating tides are triggered by interactions with planetary topography's zonal structure, thermal inertia and albedo variations (Forbes & Hagan, 2000; R. Wilson, 2000; R. J. Wilson et al., 2007).

According to different zonal wave numbers and frequencies, the atmospheric thermal tides can be expressed as the function of universal time and longitude:

$$x = A(z,\theta)\cos[n\Omega t + s\lambda + \Phi(z,\theta)] \quad (1)$$

Where n is the frequency of the oscillation (n = 1, 2 corresponds to diurnal and semidiurnal tides respectively), s is the zonal wave number (s > 0 indicates westward propagating), z is altitude, θ is latitude, t is the universal time, Ω is the planetary rotation rate, λ is the longitude, A, and φ are the amplitude and phase of the individual tidal mode. Generally, a tidal component is designated based on frequency, zonal wave number, and propagation direction. For instance, a diurnal tide propagating eastward with a zonal wave number of 2 is referred to as DE2. The expression of the tides can be represented as:

$$x = A(z,\theta)\cos[(s-n)\lambda + \Phi'(z,\theta)] \quad (2)$$

when observed within the fixed local time frame.

The tides can influence water vapor transport by driving mesospheric meridional circulation and redistributing the chemical constituents (Shaposhnikov et al., 2019; Wu et al., 2020) or influencing Jeans' escape of hydrogen into space through wave-induced perturbations in temperature and density in the thermosphere and near the exobase (Yiğit, 2021, 2023). Understanding the current state of atmospheric tides on Mars is crucial for unraveling the

coupling mechanisms from the lower Martian atmosphere to space, elucidating atmospheric escape processes, and understanding the evolution of the Martian environment.

Since Hanel et al., (1972) pioneered the study of Martian atmospheric tides through temperature observations from the Infrared Spectroscopy Experiment on Mariner 9, the characteristics of the atmospheric tides on Mars have been unveiled with subsequent observations and model studies. Forbes et al. (2002) studied the vertical propagation of nonmigrating diurnal and semidiurnal tides through the GCM model and the Global Scale Wave Model for Mars (Mars GSWM). Wilson. (2002) used density data from the Mars Global Surveyor (MGS) accelerometer to discern wave 2 and wave 3 structures in the upper atmosphere of Mars, associating them with DE2 and SE1 tides in the middle and low latitudes. Withers et al. (2011) investigate the non-migrating tides between 70 and 120 km based on data from the Spectroscopy for Investigation of Characteristics of the Atmosphere of Mars (SPICAM) ultraviolet spectrometer onboard Mars Express. Recently, the Mars Climate Sounder (MCS) instrument onboard the Mars Reconnaissance Orbiter (MRO) has implemented a multi-local time observational strategy (Kleinböhl et al., 2009), enabling concurrent measurements of atmospheric temperature and dust, which offers opportunities to ascertain the climatology and variation of the thermal tides (Lee et al., 2009; Wu et al., 2020, 2021). Forbes et al. (2020) derived the climatology of migrating (DW1, SW2) and non-migrating (DE3, DE2, DE1, SE1, S0, and SW1) tides at 76 km from Multiyear MRO/MCS measurements, the amplitude and structure of which corresponds well with those from Mars Climate Database (MCD).

The Mars Atmosphere and Volatile EvolutioN (MAVEN) mission, designed to study the structure and escape of the Martian atmosphere, provides observation of Mars's upper atmosphere and magnetosphere (Jakosky et al., 2015). Based on the temperature and density observation from stellar occultation of the Imaging Ultraviolet Spectrograph (IUVS) aboard MAVEN, recent studies investigated the diurnal tide (Gupta et al., 2022) and the wave-3 structure in the upper atmosphere on Mars (England et al., 2016; Fu et al., 2023; Lo et al., 2015; Medvedev et al., 2016). As suggested by previous work, no signatures of vertical propagating diurnal tide were discovered in Mars's upper mesosphere and thermosphere (~90 to 160 km), which are inconsistent with the MCD predictions (Gupta et al., 2022). Thus, the connection between the diurnal and semidiurnal tides in the lower atmosphere and those in the thermosphere remains unclear.

In pursuit of a deeper understanding of thermal tidal dynamics and vertical coupling across the Martian atmosphere, this study elucidates the seasonal variations and vertical structures of both migrating and non-migrating atmospheric tides from the troposphere to the thermosphere through a collaborative analysis of temperature data obtained from MRO/MCS and MAVEN/IUVS.

2 Data and Methods

2.1 MAVEN/IUVS

In this study, we derived the migrating and non-migrating tides within the upper mesosphere and thermosphere (90-160 km), utilizing stellar occultations facilitated by the IUVS instrument onboard the MAVEN spacecraft. MAVEN mission is committed to scrutinizing the contemporary conditions of the Martian upper atmosphere and ionosphere, launched in November 2013 and successfully achieving Martian orbit by October 2014. The mission is poised to enhance our understanding of atmospheric escape and the evolution of Martian climatology (Jakosky et al., 2015). The concrete working mechanism of IUVS can be referred to McClintock et al. (2015). Stellar occultation observations by the MAVEN/IUVS are executed in dedicated bimonthly "campaigns," which provide profiles of local densities, temperature, and pressure for different local times (Gröller et al., 2018; Jakosky et al., 2015; McClintock et al., 2015). Out of 3,003 occultations since March 2015, 47% occurred during the daytime, contaminated by stray light, and cannot be utilized in most analyses (Jiang et al., 2019; Nakagawa, Jain, et al., 2020; Nakagawa, Terada, et al., 2020). By utilizing an improved algorithm, Gupta et al. (2022) have broadened the data set's usability of both daytime and nighttime variations for mission-wide investigations (covering Martian years, MYs 33–36) in the Martian upper mesosphere/lower thermosphere (~90 to 160 km). This reprocessed dataset were adopted to derive the diurnal and semidiurnal tides.

2.2 MCS datasets

This study utilizes the version 5 MCS dataset from the Planetary Data System. Over eight Martian years (MYs 28–36), MCS has systematically measured thermal emissions within the

Martian atmosphere through both limb and on-planet perspectives. Operating at approximately 3 a.m./3 p.m. during 14 orbits within each sol, MCS covers an extensive latitudinal range from ~85◦S to ~85◦N. The retrieved MCS data is then interpolated across 105 vertical pressure levels, ranging from the planetary surface to ~80 km, with an effective vertical resolution of ~5 km (McCleese et al., 2007). Since September 2010, the MCS has adopted a "cross-track" observational strategy, which entails adjusting its azimuth actuator to observe the limb at angles of 90◦ to the left or right of the orbital direction or to view the limb "off-track' anywhere between 0 and 90°. For each additional azimuth angle, MRO/MCS observes one additional LT during both the ascending and descending sections of the orbit (Kleinböhl et al., 2009, 2013). Using this strategy, MRO/MCS observations span 6-8 LT per sol, targeting a solar longitude (Ls) range of 10–20° for each multi-LT sequence, except for one full year in MY 33 (Wu et al., 2020).

2.3 Fitting the tides

Through the collection of temperature observations at diverse locations during various local times, including both daytime and nighttime periods, it becomes feasible to employ fitting procedures to ascertain the amplitude and phase of the tides with different wave numbers and periods. To obtain sufficient coverage of data in the longitude and local time, we first bin the temperature profiles from MAVEN/IUVS within a solar longitude span of 60° and a latitude span of 30° from all the Martian years. Only bins meeting the following two criteria are considered for fitting distinct tidal amplitudes and phases: 1) The bin must contain observations at more than four distinct local times, covering both daytime and nighttime, with the largest gap between adjacent local times being less than 8 hours. 2) there must be six or more distinct longitude observations for a specific local time observation, and the maximum gap between adjacent longitude observations should not exceed 90°.

An example of the data binning in the longitude-LT cross-section is shown in **Figure 1a**. Within the latitude range of 15°S-15°N and the Ls range of 30°-90°, 101 temperature measurements at 130 km were recorded across six campaigns spanning from MY 33 to 36, including a broad range of longitudes and various local times during both day and night. The LT interval is smaller than 12 hours, so the diurnal and semidiurnal tides can be determined by

fitting. The significant variations in atmospheric temperatures are observed at distinct LTs within the upper mesosphere and thermosphere (**Figure 1b**), implying the activity of the diurnal tides.

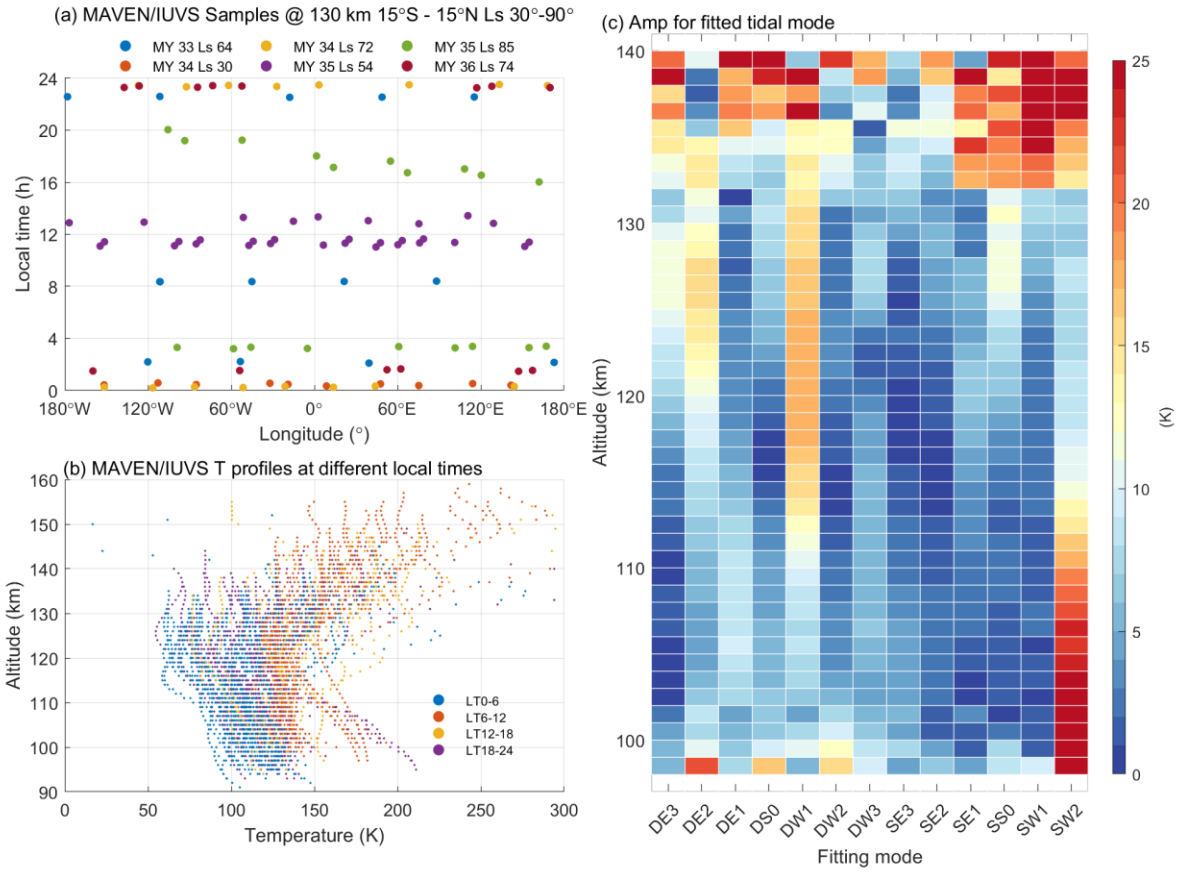

Figure 1. (a) the longitude and local time distribution of the MAVEN/IUVS sampling for temperature at 130 km from Ls 30°- 90°, latitude range of 15°S-15°N. (b) the temperature profiles at different local times and altitudes from Ls 30°- 90°. (c) Amplitude for different tide modes fitted from the temperature profiles observed by MAVEN/IUVS from Ls 30°- 90°.

The amplitude and phase of the wave in temperature are determined by harmonic fitting. Fitting results within the latitude of 15°S-15°N and Ls of 30°-90°are shown in **Figure 1c**. The seasonal variation and meridional structure of tides can be obtained by repeating the fitting process for the 2,982 bins across 7 latitude ranges, 6 Ls periods, and 81 altitudes. According to the tidal fitting experiments based on simulated sampling, the fitting from the MAVEN/IUVS sampling points can effectively capture the climatological characteristics of the diurnal and semidiurnal tides (**Figure S1**). However, MAVEN/IUVS did not cover all the LTs. Results from

bins where harmonic fitting confidence fell below 95% were excluded from subsequent analyses. Including MY 34 data with a global dust storm does affect tidal fitting near Ls=180°, especially amplitude. Still, it has little impact on the tidal phases and its seasonal variation.

In accordance with the methodology outlined by (Wu et al., 2020), the amplitude and phase of diurnal and semidiurnal tides can be derived from the temperature data observed by the MCS through a 2-dimensional nonlinear least squares fitting procedure involving local time and longitude. Figure S2 presents the observation strategies utilized by MRO/MCS, showcasing an example of the sampling points distribution and the associated tidal amplitude fitting derived from them. Additional specifics regarding the fitting methodology for the estimation of tidal information are elaborated in (Wu et al., 2022).

3 Results

As depicted in **Figure 1c**, from 100 to 130 km, DW1 and SW2 manifest notable amplitudes in 15°N-15°S during Ls=30°-90°. The DW1 attains its maximum amplitude of 15-20 K at ~120 km, coinciding with this region's day/night difference (Gupta et al., 2022). The SW2 amplitude is largest (~25 K) below 110 km and weaker above 120 km. Above 100 km, the tropical mean DE2 stands out as the third most pronounced mode besides DW1 and SW2, with the largest amplitude over 15 K at 120 km, consistent with previous studies (Fu et al., 2023). At 125-130 km, the peak amplitudes of DE3 and SS0 reach 10K. Other tidal amplitudes are below 10K at 100-130 km. The significantly increased amplitudes of multiple tidal components above 135 km are possibly due to thermospheric tidal sources or nonlinear wave interactions. Sparse sampling at higher altitudes may also lead to significant fitting errors. During other periods, DW1 and SW2 are still the dominant components. DE2 is the most active nonmigrating component, while DE3 exhibits significant amplitudes in the first half of the Martian year (**Figure S3**).

According to the theory of gravity waves, the downward phase progression indicates upward wave energy and momentum propagation. By tracking the vertical phase variation, one can estimate the vertical direction of tidal propagation and the potential altitude of the excitation source. **Figure 2** illustrates the multi-year averaged phase in the tropics (40°S-40°N) of two

migrating tides and two diurnal nonmigrating tides (DE2 and DE3) extracted from MAVEN/IUVS (90-160 km) and MRO/MCS (30-100 km) temperature observations in 6 Ls ranges. The tropical mean phase of DW1 and SW2 (green lines in **Figures 2a and 2b**) exhibit downward phase progression above 100 km, indicating the upward propagation of wave energy and momentum. The discrepancies in tidal phases between the MRO/MCS and MAVEN/IUVS datasets near 100 km may be due to spatial and temporal sampling differences. However, analyzing the phase changes with altitude allows us to infer the vertical propagation of the tides. The mean phase velocity of DW1 indicates downward propagation) within 80-100 km, which becomes more significant near Ls=60° and Ls=120°, implying a tidal source near 100 km. DW1 propagates upward from 50 to 80km during all the Ls periods.

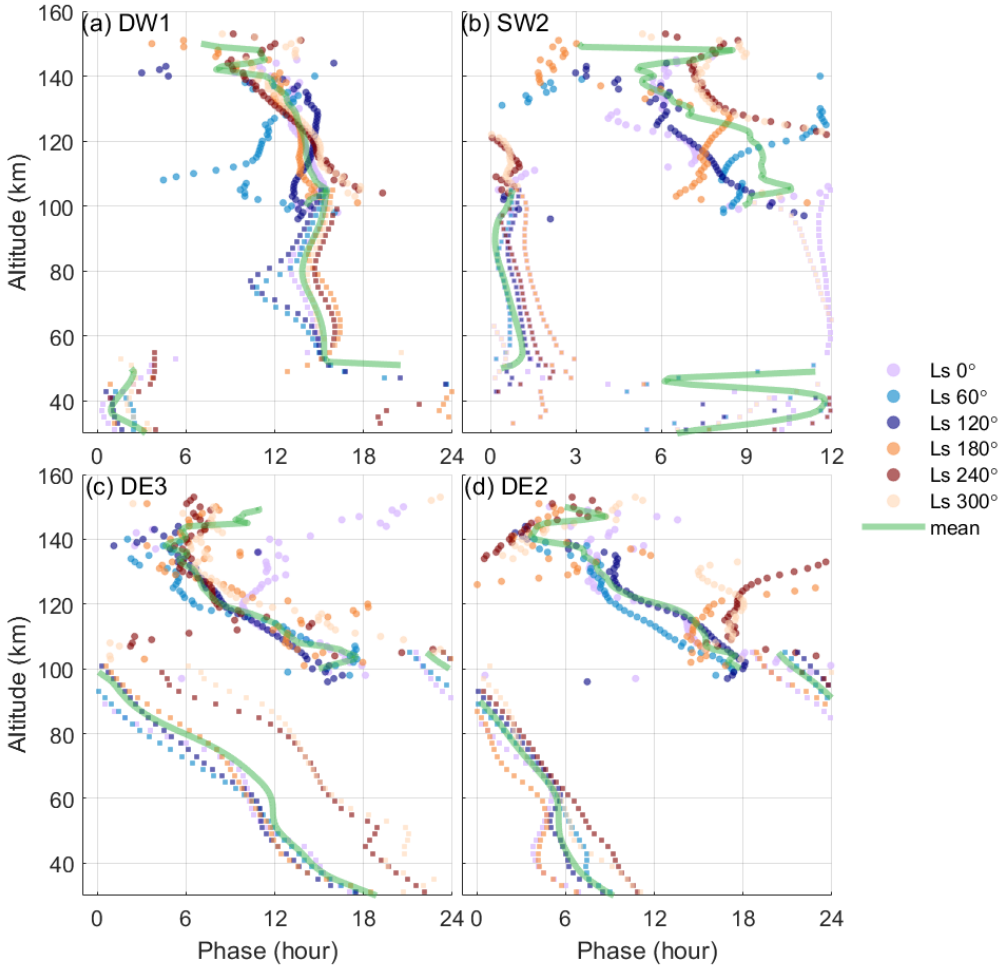

Figure 2. The vertical structure of the (a) DW1, (b) SW2, (c) DE3, (d) DE4 tidal phase in the tropics from 90 to 160 km derived from MAVEN/IUVS (dots) and from 30 to 100 km derived from MCS (bars) during MY33-MY36 at

different solar longitudes. Dots and squares of different colors represent the mean phases of MAVEN/IUVS and MRO/MCS, respectively, for the periods centered at Ls 0°, 60°, 120°, 180°, 240°, and 300°, spanning 60°. The thick green line denotes the mean phase.

Between 100 and 140 km, DW1 propagates downward during Ls=60° and Ls=120°, indicating a tidal source above 140 km, consistent with the dominant solar control over diurnal temperature variations (Gupta et al., 2022). For the Martian dusty season (Ls=180°-240°), the DW1 propagates upward from 100 km to above 140 km, suggesting the energy and momentum transport from the mesosphere to the thermosphere.

The SW2 phase varies slowly from 50 to 100 km, agreeing with classical tidal theory (Kleinböhl et al., 2013), but is more variable below 50 km. Above 100 km, the SW2 phase appears irregular near Ls=0°, implying the trapped propagation and the existence of the tidal source. At Ls=120°, SW2 can propagate upward from 100 km to 140 km but propagate downward in the thermosphere at Ls=60° and Ls=180°. At Ls=240° and Ls=300°, the SW2 is likely trapped between 100 km and 120 km but exhibits upward propagation above 120 km.

The mean phases of DE2 and DE3 suggest continuous upward propagation from 30 to 140 km (**Figures 2c** and **2d**). DE3 tides show upward propagation at 50-100 km at different Ls ranges, with disturbances at 40-60 km, likely due to the radiation absorption from water ice clouds there (Wu et al., 2021). During Ls=180°-240°, the DE3 phases shifted compared to other Ls periods below 100 km, potentially influenced by the dust activity. Above 100 km, DE3 can propagate upward to near 130 km except at the northern spring equinox (Ls=0°). However, DE3's upward propagation is suppressed above 130 km, possibly related to an extra tidal source or wave-wave interaction in the thermosphere.

The upward propagations of DE2 are clear from 30 km to 100 km in all the Ls periods. During the equinox (Ls=0° and Ls=180°), the disturbed phases between 40-60 km may be attributed to the excitation source due to water ice cloud activity. For Ls=60° and Ls=120°, DE2 directly propagates upward from 40 to ~140 km in the tropical region (**Figure 2d**), which indicates that the tidal excitation source excited by the heating or the nonlinear interaction (Forbes et al., 2020) can be traced to altitudes below 40 km. For the dust season (Ls=180° to Ls=300°), the phase of DE2 remains at LT=15 between 100 and 120 km, indicating the suppressed upward propagation of DE2. Near perihelion (Ls=240°), the DE2 phase progresses

upward from 120 to ~150 km, suggesting the excitation source of DE2 is likely located above 150 km

Generally, DW1 can propagate from the upper mesosphere (above 100 km) to the thermosphere (150 km) during the dust season, while SW2 can propagate there near Ls=120°. DE2 and DE3 exhibit upward propagation from the troposphere to the thermosphere (130-150 km) in the non-dust periods (Ls 60°-120°). However, the upward propagation of DE3 is suppressed above 130 km. Unlike the four tidal components highlighted in **Figure 2**, the vertical propagation of other diurnal and semidiurnal nonmigrating tides is not evident, as depicted in **Figure S4**. The absence of clear vertical propagation may be due to in-situ dominant thermospheric heating for these tidal components.

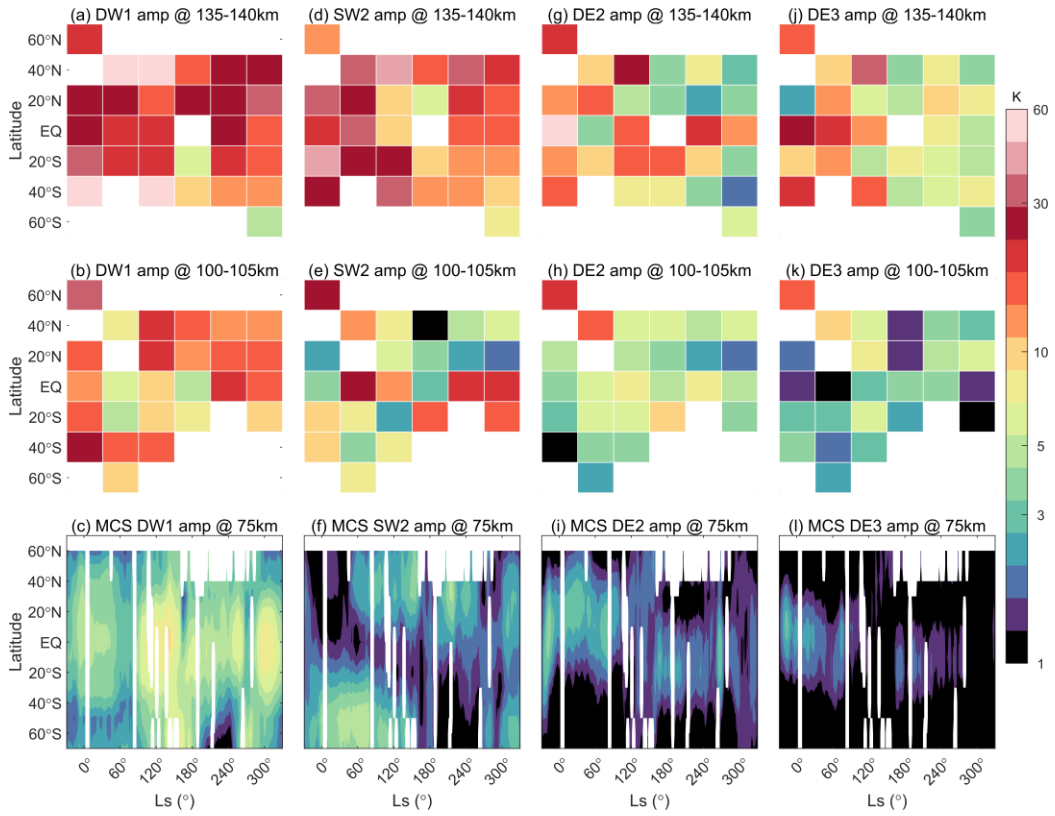

Figure 3. Seasonal variation of tidal amplitude derived from MAVEN/IUVS for DW1 (a, b), SW2 (d, f), DE2 (g, h) and DE3 (j, k) at 135-140 km (upper panel) and 100-105 km (middle panel). The amplitudes for corresponding tidal components at 75 km during MY33-MY36 derived from MCS observation are presented in the lower panel (c, f, i, l).

The variability of DW1 tidal amplitudes over latitudes and LSs throughout the Martian year is derived from multi-year MAVEN/IUVS observations at 135-140 km (**Figures 3a**) and 100-105 km (**Figures 3b)**. **Figure 3c** illustrates the seasonal variations of the DW1 mean amplitude at 75 km derived from MRO/MCS data covering MY 33 to 36 years. At 135-140 km, the DW1 amplitude from the MAVEN/IUVS is most robust in the southern hemispheric (SH) mid-latitudes near the spring equinox (Ls=0°) (**Figure 3a**). At 100-105 km, the DW1 amplitude is more significant in the middle and high latitudes near Ls=0° and is weaker from Ls=60° to Ls=180° (**Figure 3b**). At 75 km, the mesospheric DW1 from MRO/MCS exhibits greater amplitude near the equator, with two peaks observed in the Ls range of 120-180° and near 300°, respectively (**Figure 3c**). The DW1 amplitude shows inconsistent seasonal variations and meridional distributions at lower and higher altitudes, indicating that the DW1 tide in the mesosphere and thermosphere could driven by different sources, which agrees with the solar-controlled diurnal temperature variation in the thermosphere as suggested by (Gupta et al., 2022). At 100-105 km and 135-140 km（**Figures 3d and 3e)**, the SW2 amplitude attains its peak near the tropics from Ls=0° to Ls=120°, while the mesospheric SW2 is more significant in the middle and high latitudes around the winter solstices in both the NH and SH (**Figure 3f**).

Figures 3g and **3h** show that the DE2 amplitudes maximize in the NH thermosphere. The amplitudes are significantly stronger during the northern spring and summer (Ls=0° to Ls=120°) than in the northern autumn and winter (Ls=180° to Ls=300°). The seasonal and latitude pattern of mesospheric DE2 amplitude is similar to that in the thermosphere. DE3 has larger amplitudes in the first half of MY in the mesosphere (**Figures 3i)** and thermosphere (**Figures 3j** and **3k)**. The consistency in seasonal variation of DE2 and DE3 in the mesosphere and thermosphere supports their direct upward propagation from the lower atmosphere to the upper atmosphere.

Following the classical tidal theory, the latitudinal structure of a tide characterized by a specific wavenumber and period can be represented through an expansion of orthogonal Hough functions. These functions serve as eigenfunction solutions to Laplace's tidal equation (Chapman & Lindzen, 1987; Forbes et al., 2020). To further investigate the characteristics of the two propagating tidal components, the Hough decompositions are applied to their latitudinal structure from 55°S-55°N (**Figures 4a and 4e)**. The seasonal variability of amplitude for each DE2 and DE3 Hough mode from 110 km to 130 km is presented in **Figures 4b and 4f**. Due to insufficient

MAVEN/IUVS data in the range of Ls 330° to 30° between 25°N and 55°N, a Hough decomposition was not performed for the tides during this period.

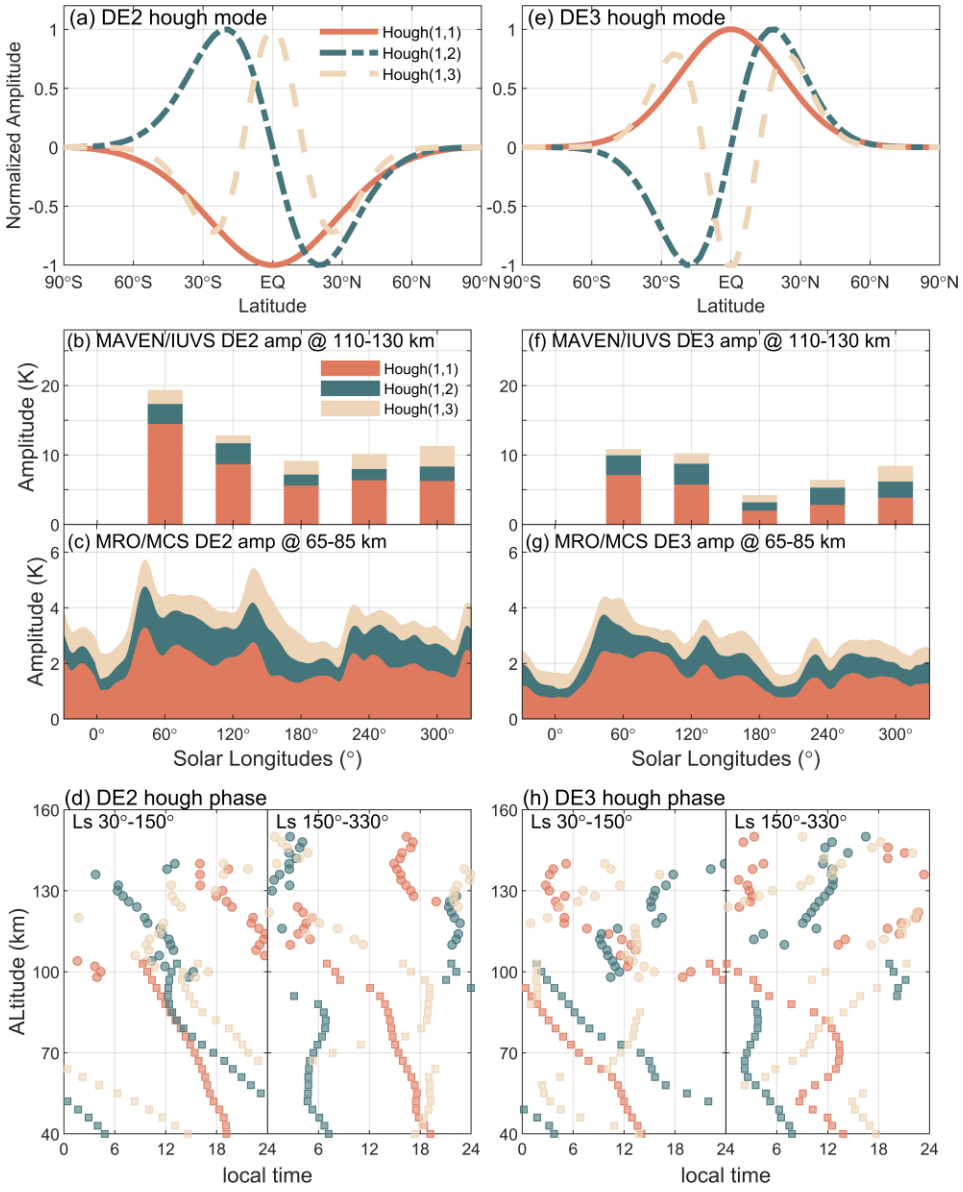

Figure 4. The first three Hough modes of (a) DE2; the amplitudes for the first three DE2 Hough modes at (b) 110-130 km from MAVEN/IUVS and (c) at 65-85 km from MRO/MCS at different Ls periods (each corresponds to a 60° Ls span); (d) the mean phase for DE2 Hough modes for Ls=30°-150° and Ls=150°-330° from MAVEN/IUVS (dots) and from MRO/MCS (squares). (e)-(h) the same as (a)-(d) but for DE3 tide.

The Hough (1,1) mode governs the seasonal variation of DE2 in both the mesosphere and thermosphere. In the thermosphere, DE2 (1, 1) amplitude is largest (~15K) at Ls= 60° and decreases to ~5 K at Ls=180°-300°, which corresponds with the mesospheric pattern at 65-85 km **(Figure 4c)**. The DE2 (1, 2) is also stronger in the first half of MY but weaker in the second half

in both layers. The thermospheric DE2 (1,3) mode is the weakest during Ls=120° (~1 K) and is the strongest during Ls=300° (~3 K), while its mesospheric counterpart has no significant seasonal variation. The variation of DE3 is also controlled by the Hough (1,1) mode, the seasonal variation of which is similar in the thermosphere and mesosphere. **(Figure 4f and 4g)**.

Given that both DE2 and DE3 exhibit stronger amplitudes in the first half of MY (Ls=60° and Ls=120°) and weaker amplitudes in the latter half (Ls=180° to Ls=300°), we further investigate their vertical propagation characteristics by examining the phase of different Hough modes during these periods **(Figures 4d and 4h)**. From Ls=30° to Ls=150°, the DE2 (1, 1) and (1,2) modes propagate upward continuously from 40 km to approximately 140 km, while the (1,3) mode is trapped above 100 km. For the DE3 tide, both (1,1) and (1,2) modes propagate upward below 100 km, while only (1,1) modes can propagate vertically to above 130 km. DE3 (1,3) mode cannot propagate vertically in either the mesosphere or the thermosphere. Both the stronger amplitudes in the mesosphere and the vertical propagating features of DE2 and DE3 contribute to the larger amplitudes in the thermosphere in this period.

During the second half of MY, the hough (1,1) and (1, 2) modes of DE2 are trapped above 100 km, while the (1, 3) mode propagates upward until 130 km. As a result, the DE2 (1, 3) becomes stronger in the thermosphere, although its amplitude remains unchanged in the mesosphere. All three Hough modes of DE3 are trapped during the second half of MY.

4 Summary and Discussion

This study utilized temperature data observed by MAVEN/IUVS, including both daytime and nighttime data from 90 to 160 km, and the data with multi-LT observation by the “off-track/cross-track” strategy of MRO/MCS below 100 km to derive the migrating and nonmigrating diurnal and semidiurnal tidal components. As previous studies have focused more on non-migrating tides, this study also discussed the characteristics of the migrating tides. The investigation of vertical phase velocities revealed that during the dust season (Ls=240° and Ls=300°), the tropical average DW1 and SW2 tides propagate upward since 100 km. DE2 and DE3 can propagate upward from below 40 km continuously to 130-140 km during the “non-dust” season (Ls=0°-150°), suggesting tidal excitations originate from the lower atmosphere. However, these nonmigrating tides become trapped above 100 km during the “dust” season (Ls=180° and 240°). The amplitude variations and vertical propagation of the Hough (1,1) modes primarily

control the seasonal variations of DE2 and DE3 in both mesosphere and thermosphere. The vertical propagation characteristics of tides other than DW1, SW2, DE2, and DE3 are not significant.

By comparing the seasonal variations and zonal distribution of the lower atmospheric tides extracted from temperature observation by MRO/MCS, the seasonal variation of DE2 and DE3 tidal amplitudes in the thermosphere agree with its mesospheric counterpart. In contrast, significant differences exist in the zonal distribution and seasonal variations of DW1 and SW2 amplitudes between the mesosphere and thermosphere. The lack of evident vertical propagation in some tides may be due to multiple tidal sources in the mesosphere and thermosphere, associated with the distribution of dust, water, CO2, and the radiative balance between direct solar UV heating and infrared emission cooling, or be affected by the non-linear interactions of stronger tides. These mechanisms could also contribute to the suppressed upward propagation of DW1, SW2, DE2, and DE3.

In conclusion, our findings indicate that specific thermal migrating (DW1 and SW2) and non-migrating tides (DE2 and DE3) on Mars can propagate upward among specific altitude ranges. The upward propagation facilitates the energy and momentum transfer from the lower to the upper atmosphere, potentially influencing the vertical coupling across the entire Martian atmosphere (Wu et al., 2022; Yiğit, 2021).

Acknowledgments

This work was supported by the B-type Strategic Priority Program of the Chinese Academy of Sciences, Grant XDB41000000; the National Natural Science Foundation of China grants (42241115, 42275133, 42130203, 42241135); the National Key R\&D Program of China (Grant No. 2022YFF0503703).

Open Research

Data Availability Statement

The MAVEN/IUVS calibrated (level 1B) stellar occultation data (Schneider, 2022) are publicly available in FITS format on the NASA Planetary Data System (PDS) at

https://atmos.nmsu.edu/PDS/data/PDS4/MAVEN/iuvs_ calibrated_bundle/l1b/occultation/, identified by "occultation" with version/revision tag v13_r01. Data used in this study, can be downloaded from the CU Scholar data repository (Gupta, 2022) at https://scholar.colorado.edu/concern/datasets/h702q775d. The MCS data used in this study are available for download at https://pds-atmospheres.nmsu.edu/data_ and_services/atmospheres_data/MARS/atmosphere_temp_prof.html. The derived diurnal and semidiurnal tidal amplitude and phase from MAVEN/IUVS and MRO/MCS can be accessed on OSF repository (Yang, 2023).

References

Angelats I Coll, M., Forget, F., López-Valverde, M. A., Read, P. L., & Lewis, S. R. (2004). Upper atmosphere of Mars up to 120 km: Mars Global Surveyor accelerometer data analysis with the LMD general circulation model. *Journal of Geophysical Research: Planets*, *109*(E1), 2003JE002163. https://doi.org/10.1029/2003JE002163

Chapman, S., & Lindzen, R. S. (1987). *Atmospheric tides: Thermal and gravitational*. Gordon and Breach ; D. Reidel.

England, S. L., Liu, G., Kumar, A., Mahaffy, P. R., Elrod, M., Benna, M., Jain, S., Deighan, J., Schneider, N. M., McClintock, W. E., & Evans, J. S. (2019). Atmospheric Tides at High Latitudes in the Martian Upper Atmosphere Observed by MAVEN and MRO. *Journal of Geophysical Research: Space Physics*, *124*(4), 2943–2953. https://doi.org/10.1029/2019JA026601

England, S. L., Liu, G., Withers, P., Yiğit, E., Lo, D., Jain, S., Schneider, N. M., Deighan, J., McClintock, W. E., Mahaffy, P. R., Elrod, M., Benna, M., & Jakosky, B. M. (2016). Simultaneous observations of atmospheric tides from combined in situ and remote observations at Mars from the MAVEN spacecraft. *Journal of Geophysical Research: Planets*, *121*(4), 594–607. https://doi.org/10.1002/2016JE004997

Forbes, J. M. (2004). Tides in the middle and upper atmospheres of Mars and Venus. *Advances in Space Research*, *33*(2), 125–131. https://doi.org/10.1016/j.asr.2003.05.007

Forbes, J. M. (2013). Tidal and Planetary Waves. In R. M. Johnson & T. L. Killeen (Eds.), *Geophysical Monograph Series* (pp. 67–87). American Geophysical Union. https://doi.org/10.1029/GM087p0067

Forbes, J. M., Bridger, A. F. C., Bougher, S. W., Hagan, M. E., Hollingsworth, J. L., Keating, G. M., & Murphy, J. (2002). Nonmigrating tides in the thermosphere of Mars. *Journal of Geophysical Research: Planets*, *107*(E11). https://doi.org/10.1029/2001JE001582

Forbes, J. M., & Hagan, M. E. (2000). Diurnal Kelvin wave in the atmosphere of Mars: Towards an understanding of 'stationary' density structures observed by the MGS accelerometer. *Geophysical Research Letters*, *27*(21), 3563–3566. https://doi.org/10.1029/2000GL011850

Forbes, J. M., Zhang, X., Forget, F., Millour, E., & Kleinböhl, A. (2020). Solar Tides in the Middle and Upper Atmosphere of Mars. *Journal of Geophysical Research: Space Physics*, *125*(9), e2020JA028140. https://doi.org/10.1029/2020JA028140

Fu, M., Ren, Z., Cui, J., Zhou, X., Wu, Z., & Fan, K. (2023). Atmospheric Tides at Low Latitudes in the Martian Upper Atmosphere Observed by MAVEN IUVS. *Journal of Geophysical Research: Space Physics*, *128*(10), e2023JA032016. https://doi.org/10.1029/2023JA032016

Gröller, H., Montmessin, F., Yelle, R. V., Lefèvre, F., Forget, F., Schneider, N. M., Koskinen, T. T., Deighan, J., & Jain, S. K. (2018). MAVEN/IUVS Stellar Occultation Measurements of Mars Atmospheric Structure and Composition. *Journal of Geophysical Research: Planets*, *123*(6), 1449–1483. https://doi.org/10.1029/2017JE005466

Gupta, S. (2022). *Thermal Structure of the Martian Upper Mesosphere/Lower Thermosphere from MAVEN/IUVS Stellar Occultations [Data]* [dataset]. [object Object]. https://doi.org/10.25810/Z1WY-CQ62

Gupta, S., Yelle, R. V., Schneider, N. M., Jain, S. K., González-Galindo, F., Verdier, L., Braude, A. S., Montmessin, F., Mayyasi, M., Deighan, J., & Curry, S. (2022). Thermal Structure of the Martian Upper Mesosphere/Lower Thermosphere From MAVEN/IUVS Stellar Occultations. *Journal of Geophysical Research: Planets*, *127*(11). https://doi.org/10.1029/2022JE007534

Hanel, R., Conrath, B., Hovis, W., Kunde, V., Lowman, P., Maguire, W., Pearl, J., Pirraglia, J., Prabhakara, C., Schlachman, B., Levin, G., Straat, P., & Burke, T. (1972). Investigation of the Martian environment by infrared spectroscopy on Mariner 9. *Icarus*, *17*(2), 423–442. https://doi.org/10.1016/0019-1035(72)90009-7

Jakosky, B. M., Lin, R. P., Grebowsky, J. M., Luhmann, J. G., Mitchell, D. F., Beutelschies, G., Priser, T., Acuna, M., Andersson, L., Baird, D., Baker, D., Bartlett, R., Benna, M., Bougher, S., Brain, D., Carson, D., Cauffman, S., Chamberlin, P., Chaufray, J.-Y., … Zurek, R. (2015). The Mars Atmosphere and Volatile

Evolution (MAVEN) Mission. *Space Science Reviews*, *195*(1–4), 3–48. https://doi.org/10.1007/s11214-015-0139-x

Jiang, F. Y., Yelle, R. V., Jain, S. K., Cui, J., Montmessin, F., Schneider, N. M., Deighan, J., Gröller, H., & Verdier, L. (2019). Detection of Mesospheric CO_2 Ice Clouds on Mars in Southern Summer. *Geophysical Research Letters*, *46*(14), 7962–7971. https://doi.org/10.1029/2019GL082029

Kleinböhl, A., John Wilson, R., Kass, D., Schofield, J. T., & McCleese, D. J. (2013). The semidiurnal tide in the middle atmosphere of Mars: FRONTIER. *Geophysical Research Letters*, *40*(10), 1952–1959. https://doi.org/10.1002/grl.50497

Kleinböhl, A., Schofield, J. T., Kass, D. M., Abdou, W. A., Backus, C. R., Sen, B., Shirley, J. H., Lawson, W. G., Richardson, M. I., Taylor, F. W., Teanby, N. A., & McCleese, D. J. (2009). Mars Climate Sounder limb profile retrieval of atmospheric temperature, pressure, and dust and water ice opacity. *Journal of Geophysical Research: Planets*, *114*(E10), 2009JE003358. https://doi.org/10.1029/2009JE003358

Lee, C., Lawson, W. G., Richardson, M. I., Heavens, N. G., Kleinböhl, A., Banfield, D., McCleese, D. J., Zurek, R., Kass, D., Schofield, J. T., Leovy, C. B., Taylor, F. W., & Toigo, A. D. (2009). Thermal tides in the Martian middle atmosphere as seen by the Mars Climate Sounder. *Journal of Geophysical Research: Planets*, *114*(E3), 2008JE003285. https://doi.org/10.1029/2008JE003285

Lo, D. Y., Yelle, R. V., Schneider, N. M., Jain, S. K., Stewart, A. I. F., England, S. L., Deighan, J. I., Stiepen, A., Evans, J. S., Stevens, M. H., Chaffin, M. S., Crismani, M. M. J., McClintock, W. E., Clarke, J. T., Holsclaw, G. M., Lefèvre, F., & Jakosky, B. M. (2015). Nonmigrating tides in the Martian atmosphere as observed by MAVEN IUVS. *Geophysical Research Letters*, *42*(21), 9057–9063. https://doi.org/10.1002/2015GL066268

McCleese, D. J., Schofield, J. T., Taylor, F. W., Calcutt, S. B., Foote, M. C., Kass, D. M., Leovy, C. B., Paige, D. A., Read, P. L., & Zurek, R. W. (2007). Mars Climate Sounder: An investigation of thermal and water vapor structure, dust and condensate distributions in the atmosphere, and energy balance of the polar regions. *Journal of Geophysical Research: Planets*, *112*(E5), 2006JE002790. https://doi.org/10.1029/2006JE002790

McClintock, W. E., Schneider, N. M., Holsclaw, G. M., Clarke, J. T., Hoskins, A. C., Stewart, I., Montmessin, F., Yelle, R. V., & Deighan, J. (2015). The Imaging Ultraviolet Spectrograph (IUVS) for the MAVEN Mission. *Space Science Reviews*, *195*(1–4), 75–124. https://doi.org/10.1007/s11214-014-0098-7

Medvedev, A. S., Nakagawa, H., Mockel, C., Yiğit, E., Kuroda, T., Hartogh, P., Terada, K., Terada, N., Seki, K., Schneider, N. M., Jain, S. K., Evans, J. S., Deighan, J. I., McClintock, W. E., Lo, D., & Jakosky, B. M. (2016). Comparison of the Martian thermospheric density and temperature from IUVS/MAVEN data and general circulation modeling. *Geophysical Research Letters*, *43*(7), 3095–3104. https://doi.org/10.1002/2016GL068388

Moudden, Y., & Forbes, J. M. (2015). Density prediction in Mars' aerobraking region. *Space Weather*, *13*(1), 86–96. https://doi.org/10.1002/2014SW001121

Nakagawa, H., Jain, S. K., Schneider, N. M., Montmessin, F., Yelle, R. V., Jiang, F., Verdier, L., Kuroda, T., Yoshida, N., Fujiwara, H., Imamura, T., Terada, N., Terada, K., Seki, K., Gröller, H., & Deighan, J. I. (2020). A Warm Layer in the Nightside Mesosphere of Mars. *Geophysical Research Letters*, *47*(4), e2019GL085646. https://doi.org/10.1029/2019GL085646

Nakagawa, H., Terada, N., Jain, S. K., Schneider, N. M., Montmessin, F., Yelle, R. V., Jiang, F., Verdier, L., England, S. L., Seki, K., Fujiwara, H., Imamura, T., Yoshida, N., Kuroda, T., Terada, K., Gröller, H., Deighan, J., & Jakosky, B. M. (2020). Vertical Propagation of Wave Perturbations in the Middle Atmosphere on Mars by MAVEN/IUVS. *Journal of Geophysical Research: Planets*, *125*(9), e2020JE006481. https://doi.org/10.1029/2020JE006481

Shaposhnikov, D. S., Medvedev, A. S., Rodin, A. V., & Hartogh, P. (2019). Seasonal Water "Pump" in the Atmosphere of Mars: Vertical Transport to the Thermosphere. *Geophysical Research Letters*, *46*(8), 4161–4169. https://doi.org/10.1029/2019GL082839

Wilson, R. (2000). The Martian Atmosphere During the Viking Mission, I Infrared Measurements of Atmospheric Temperatures Revisited. *Icarus*, *145*(2), 555–579. https://doi.org/10.1006/icar.2000.6378

Wilson, R. J. (2002). Evidence for nonmigrating thermal tides in the Mars upper atmosphere from the Mars Global Surveyor Accelerometer Experiment. *Geophysical Research Letters*, *29*(7). https://doi.org/10.1029/2001GL013975

Wilson, R. J., Neumann, G. A., & Smith, M. D. (2007). Diurnal variation and radiative influence of Martian water ice clouds. *Geophysical Research Letters*, *34*(2), 2006GL027976. https://doi.org/10.1029/2006GL027976

Withers, P., Pratt, R., Bertaux, J.-L., & Montmessin, F. (2011). Observations of thermal tides in the middle atmosphere of Mars by the SPICAM instrument. *Journal of Geophysical Research*, *116*(E11), E11005. https://doi.org/10.1029/2011JE003847

Wu, Z., Li, T., Heavens, N. G., Newman, C. E., Richardson, M. I., Yang, C., Li, J., & Cui, J. (2022). Earth-like thermal and dynamical coupling processes in the Martian climate system. *Earth-Science Reviews*, *229*, 104023. https://doi.org/10.1016/j.earscirev.2022.104023

Wu, Z., Li, T., Li, J., Yang, C., & Cui, J. (2022). Diurnal Variations of Water Ice in the Martian Atmosphere Observed by Mars Climate Sounder. *Remote Sensing*, *14*(9), 2235. https://doi.org/10.3390/rs14092235

Wu, Z., Li, T., Li, J., Zhang, X., Yang, C., & Cui, J. (2021). Abnormal Phase Structure of Thermal Tides During Major Dust Storms on Mars: Implications for the Excitation Source of High-altitude Water Ice Clouds. *Journal of Geophysical Research: Planets*, *126*(4), e2020JE006758. https://doi.org/10.1029/2020JE006758

Wu, Z., Li, T., Zhang, X., Li, J., & Cui, J. (2020). Dust tides and rapid meridional motions in the Martian atmosphere during major dust storms. *Nature Communications*, *11*(1), 614. https://doi.org/10.1038/s41467-020-14510-x

Yang, C. (2023). *Martian atmospheric tides revealed from MAVEN and MCS Observations*. https://doi.org/10.17605/OSF.IO/S8XU5

Yiğit, E. (2021). Martian water escape and internal waves. *Science*, *374*(6573), 1323–1324. https://doi.org/10.1126/science.abg5893

Yiğit, E. (2023). Coupling and interactions across the Martian whole atmosphere system. *Nature Geoscience*, *16*(2), 123–132. https://doi.org/10.1038/s41561-022-01118-7